Palaeogeography, Palaeoclimatology, Palaeoecology 435 (2015) 127–135

Contents lists available at ScienceDirect

Palaeogeography, Palaeoclimatology, Palaeoecology

journal homepage: www.elsevier.com/locate/palaeo

Reconciliation of hydroclimate sequences from the Chinese Loess Plateau and low-latitude East Asian Summer Monsoon regions over the past 14,500 years

Jinguo Dong [a,b,*], Chuan-Chou Shen [c,**], Xinggong Kong [d], Hao-Cheng Wang [c], Xiuyang Jiang [e]

[a] College of Geosciences, Nantong University, Nantong 226007, PR China
[b] State Key Laboratory of Loess and Quaternary Geology, Institute of Earth Environment, Chinese Academy of Sciences, Xi'an 710075, PR China
[c] High-Precision Mass Spectrometry and Environment Change Laboratory (HISPEC), Department of Geosciences, National Taiwan University, Taipei 106, Taiwan ROC
[d] College of Geosciences, Nanjing Normal University, Nanjing 210097, PR China
[e] Key Laboratory of Humid Subtropical Eco-geographical Process, College of Geosciences, Fujian Normal University, Fuzhou 35000, PR China

ARTICLE INFO

Article history:
Received 18 November 2014
Received in revised form 24 May 2015
Accepted 9 June 2015
Available online 16 June 2015

Keywords:
Chinese Loess Plateau
Northern China
East Asian Summer Monsoon
Stalagmite
Regional synchronicity

ABSTRACT

We discuss replicated stalagmite $\delta^{18}O$ records with interannual-to-multidecadal resolution from Lianhua Cave on the Chinese Loess Plateau to illustrate the precipitation history of the East Asian Summer Monsoon (EASM) region over the last 14.5 thousand years (ka BP, before 1950 CE, hereafter), and to re-evaluate the inconsistency in the proxy-inferred palaeoclimate time series in northern China. Agreement between the stalagmite $\delta^{18}O$ from Lianhua and other caves from central-southern China indicates that regional climate changes after the Last Glacial were concurrent across mainland China, indicating that insolation was the primary factor controlling the evolution of the Asian Summer Monsoon (ASM). The stalagmite ^{18}O enrichment of 2.5‰ in the Younger Dryas and 1.7‰ during the 8.2-ka BP event in Lianhua were larger than those in caves from central and southern China. The evidence suggests that different meridional responses of weak precipitation conditions in the ASM realm occurred during these two abrupt events, driven by high-latitude forcing in the Northern Hemisphere. The heterogeneous hydroclimate sequences in northern China inferred from different natural archives are most likely attributable to the complexity of the formations and/or some chronological uncertainty.

1. Introduction

The East Asian Summer Monsoon (EASM) is an integral part of the Asian Summer Monsoon (ASM) system, providing the majority of rainfall to the most densely populated areas of China. The hydroclimate in the Chinese Loess Plateau (CLP), located in northern China, is associated with the EASM variability (*e.g.*, Xiao et al., 2002; Li et al., 2004; Chen et al., 2006; Zhao et al., 2013). An intensification in the southerly monsoonal airflow results in an extension of the rainfall belt into the arid interior of the continent and a complementary reduction in desert coverage in northern China (*e.g.*, Liu and Ding, 1998; Yang and Scuderi, 2010; Lu et al., 2013). This induced environmental change has dominated the regional ecological system (*e.g.*, Li et al., 2004; Zhao et al., 2009) and has also affected the rise of civil practices, such as agriculture (Li et al., 2009) and human society (*e.g.*, Zhang et al., 2008). Over recent decades, diverse natural archives, including loess (Xiao et al., 2002; Sun et al., 2010), aeolian deposits (Yang and Scuderi, 2010), lacustrine sediments (Shen et al., 2005), and speleothems (Dykoski et al., 2005; Sinha et al., 2005; Wang et al., 2005; Hu et al., 2008; Cai et al., 2010; Dong et al., 2010; Ma et al., 2012; Lone et al., 2014; Zhang et al., 2014; Cai et al., 2015) have been used to improve our understanding of the evolution of regional climates since the previous deglaciation period to aid water resource management and the establishment of a sustainability policy.

Based on radiocarbon and optically stimulated luminescence (OSL) dating, Wang et al. (2010) summarised previous lake and loess records to show that Holocene hydroclimatic changes in northern China were asynchronous with the southern EASM regions. Recent loess and dune proxy records from northern China suggest that the onset of wet climatic conditions after the Last Glacial period occurred several thousand years after the summer insolation peak at 10–11 ka BP (Xiao et al., 2002, 2004; Lu et al., 2005; Sun et al., 2006; Lu et al., 2013). However, their suggestions are challenged by the stalagmite records from southern and central China (Dykoski et al., 2005; Dong et al., 2010) and CLP lake records (Jin et al., 2004; Li et al., 2004; Jiang et al., 2006, 2009). These records suggest a direct monsoonal response to insolation forcing during the Early Holocene. Although millennial-scale changes in the EASM responded rapidly to changes in the North Atlantic climate during

* Correspondence to: J. Dong, College of Geosciences, Nantong University, Nantong, China. Tel.: +86 13626278364; fax: +86 513 85015880.
** Correspondence to: C.-C. Shen, Department of Geosciences, National Taiwan University, Taipei, Taiwan ROC. Tel.: +886 2 33662918; fax: +866 2 33636095.
E-mail addresses: dongjinguo1111@163.com (J. Dong), river@ntu.edu.tw (C.-C. Shen).

http://dx.doi.org/10.1016/j.palaeo.2015.06.013
0031-0182/

the 8.2 ka BP event and the Younger Dryas (YD) (*e.g.*, Chen et al., 2001; Ma et al., 2012; Y. Liu et al., 2013; D. Liu et al., 2013), their nature across the entire extent of monsoonal China is not well understood. For example, two stalagmite records from Dongge Cave in southern China (Wang et al., 2005; Cheng et al., 2009) show an obvious $\delta^{18}O$ anomaly occurring at 8.4–8.1 ka BP, which is also recorded in the Heshang Cave in central China (Y. Liu et al., 2013). Stalagmite $\delta^{18}O$ sequences from the Sanbao Cave in central China and the Nuanhe Cave in north-eastern China do not register this event (Dong et al., 2010; Wu et al., 2012). Hong et al. (2010) and Stebich et al. (2010) argued that a change in EASM precipitation during the YD remains an open question. Hong et al. (2005) used the Hani (42°13′N, 126°31′E) peat cellulose carbon stable isotope record to propose enhanced precipitation in northern China during the YD. However, this implication was not supported by high-resolution pollen records, which show a reversal of climatic conditions in Lake Sihailongwan (Stebich et al., 2009), located ~15 km northeast of the Hani site. Building more detailed palaeorecords for northern China, with improved timeframes, is critically important for clarifying the evolution of the regional hydroclimate.

In this study, we first built a new absolute-dated multidecadal-resolved oxygen isotope time series using three stalagmites collected from Lianhua Cave for the CLP. The composite Lianhua $\delta^{18}O$ record was compared with previous well-dated stalagmite sequences to show the synchronicity of regional precipitation variations since the Last Glaciation over the entire monsoonal region. We showed the variable meridional impact of the high-latitude forcing originating in the North Atlantic on the regional hydrology during the YD and the 8.2-ka BP event. Finally, we propose possible causes for the lack of concurrence in the proxy-inferred CLP hydroclimate sequences.

2. Cave site and samples

Lianhua Cave (38°10′N, 113°43′E), at an elevation of 1200 m, is located on the CLP, Shanxi Province, northern China (Fig. 1). The temperature (1985–2004 CE) varies from −2.5 °C in winter to 28 °C in summer (Fig. 2), recorded at the nearest meteorological station, Shijiazhuang (elevation 80 m), located 80 km east of the cave (Fig. 1). The mean annual precipitation is 530 mm (Fig. 2). This site is in an arid–semiarid zone in the northern margins of the EASM region (Yamanaka et al., 2004), with distinctive wet summers and dry winters. More than 81% (1985–2004 CE) of annual precipitation falls in summer, from May to September. The inflow of warm/humid air delivered by the EASM extends north-westerly into the interior as far as the China–Mongolia border. In winter, the southward-migrating Siberian High cold, dry air mass dominates the regional climate.

Lianhua Cave, with a small entrance 0.5 m in width and 0.5 m in height, is 200 m in length and overlain by ~50 m of Ordovician limestone of the Ma-Jia-Gou Group (Qian, 1960). The temperature in the cave is 11 °C. The humidity in the innermost tunnel is 95% on average, where three calcite stalagmites located 20–30 m apart (LH4, LH5, and LH9) were collected. Stalagmites were halved and polished for ^{230}Th dating and oxygen/carbon stable isotope analysis (Fig. 3).

3. Methods

Twenty-seven subsamples from the three collected stalagmites (15 subsamples from LH4, eight subsamples from LH5, and four subsamples from LH9, 100–200 mg each) were drilled for U–Th chemistry (Shen et al., 2003) and ^{230}Th dating (Shen et al., 2002, 2012) (Fig. 3). Uranium–thorium isotopic measurements were performed using a multi-collection inductively coupled plasma mass spectrometer (MC-ICP-MS,) Thermo Finnigan Neptune, in the High-Precision Mass Spectrometry and Environment Change Laboratory (HISPEC), Department of Geosciences, National Taiwan University (Shen et al., 2012). A gravimetrically calibrated (Cheng et al., 2013) triple-spike, ^{229}Th–^{233}U–^{236}U, isotope dilution method was employed to correct any mass bias and to determine the U–Th content and isotopic composition (Shen et al., 2012). All date errors are given to two standard deviations, unless otherwise noted.

Based on the obvious changes in lithology of the polished sections of stalagmites LH4, LH5, and LH9 (Fig. 3), six subsamples were obtained along the central growth axis of each stalagmite, and these were analysed using x-ray diffraction (XRD) on a powder diffractometer, Rigaku D/Max-2500VL/PC, located at the Institute of Testing Service Center, Nanjing Normal University, China. The XRD measurements indicate that the three stalagmites are all composed of calcite, and the mineralogical composition is homogeneous throughout the growth period (Fig. 4a).

For stable isotopic measurements, 829 subsamples, 10–20 μg each, were drilled using a 0.3 mm diameter carbide dental burr at 1 mm intervals, except for 0.5 mm intervals at depths from 139 to 155 mm in stalagmite LH4. The corresponding temporal resolution was 4–47 years. Five coeval subsamples from five horizons were selected arbitrarily from LH4 and LH5 and subjected to the "Hendy Test" (Hendy, 1971) to evaluate the oxygen isotopic equilibrium conditions during calcite

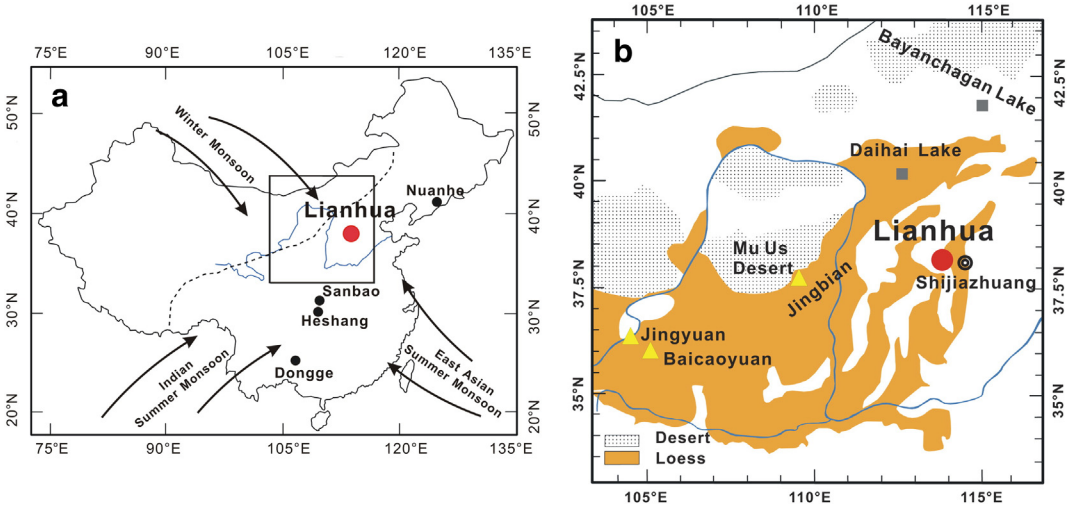

Fig. 1. (a) Location of Nuanhe (Wu et al., 2012), Lianhua (this study, red circle), Sanbao (Dong et al., 2010), Heshang (Hu et al., 2008), and Dongge (Wang et al., 2005) caves. The arrows show the modern monsoonal system in China, including the East Asian and Indian summer and winter monsoons. The dashed line denotes the averaged present-day limit of the summer monsoon. **(b)** An enlarged regional CLP map (32.9–43.7°N, 103.4–117.0°E) with desert (dotted areas), loess (triangles), and lake (squares) sites.

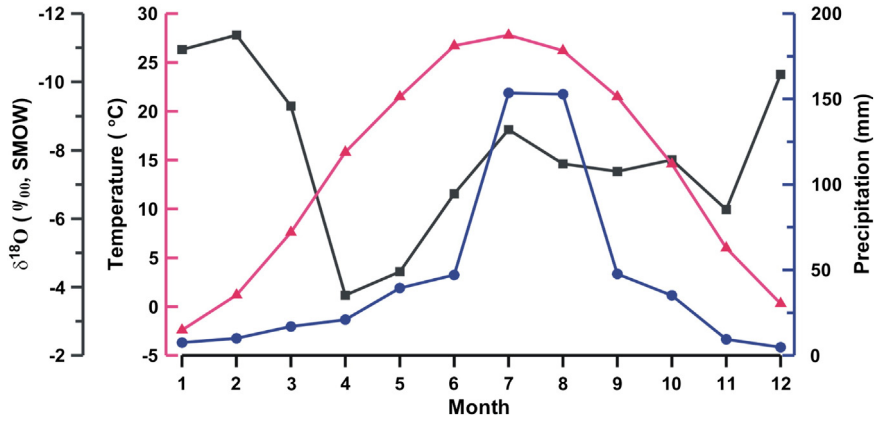

Fig. 2. Average monthly air temperature (pink), precipitation (blue), and rainfall $\delta^{18}O$ (black) in the Shijiazhuang station during 1985–2004 CE (from the Global Network of Isotopes in Precipitation (GNIP) database, http://www-naweb.iaea.org/napc/ih/IHS_resources_gnip.html).

precipitation. The analysis was conducted using two Finnigan-MAT 253 mass spectrometers equipped with an automatic Kiel carbonate device located at the College of Geosciences, Nanjing Normal University, China, and the College of Geosciences, Fujian Normal University, China. The carbonate $\delta^{18}O$ (‰) and $\delta^{13}C$ (‰) values are expressed relative to the Vienna Pee Dee Belemnite (VPDB) reference standard. An international standard, NBS-19, was measured every 15–20 samples on both mass spectrometers to confirm that 6 months 1 σ external errors were better than ±0.06‰ for $\delta^{18}O$ and ±0.1‰ for $\delta^{13}C$.

4. Results

4.1. Chronology

The uranium–thorium isotopic compositions and ^{230}Th dates obtained are shown in Table 1. All dates with an uncertainty of 1–2% were in stratigraphic order. The age–depth plots for all the stalagmites are shown in Fig. 5. A linear interpolation between the ^{230}Th dates was used to build the age models in order to directly compare with previously published records that utilised the same chronological method. The chronologies show that stalagmite LH4 grew between 14.5 and 6.0 ka BP with a hiatus at 11.2–9.8 ka BP, that stalagmite LH9 was deposited continuously from 4.5 to 1.3 ka BP, and that stalagmite LH5 was deposited from 11.6 to 3.4 ka BP, excluding two hiatuses between 8.7 and 6.8 ka BP, and 4.9 and 3.8 ka BP. The calculated growth rates were 19–183 μm/year for LH4, 30–109 μm/year for LH5, and 28–39 μm/year for LH9.

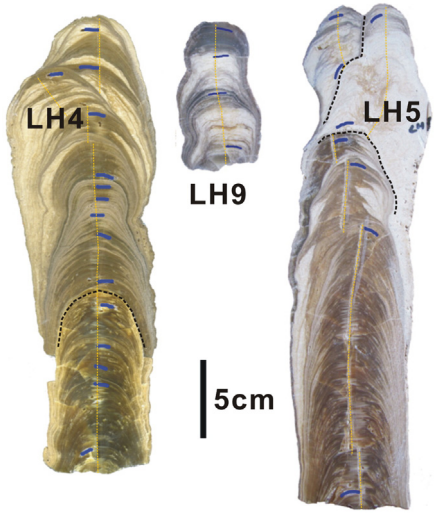

Fig. 3. Images of the three stalagmites, LH4, LH5, and LH9, collected from Lianhua Cave. Subsamples (blue) were drilled for ^{230}Th dating. Powdered subsamples were extracted along the central growth axis on the polished surface for $\delta^{18}O$ analysis (yellow dotted lines). The black dashed lines show the hiatuses in stalagmites LH4 and LH5.

4.2. Oxygen isotope records

The $\delta^{18}O$ and $\delta^{13}C$ coeval subsample datasets from five layers of two stalagmites (LH4 and LH5) are shown in Fig. 4. The 2σ variability of only ±0.06–0.12‰ for the coeval subsample $\delta^{18}O$ data (Fig. 4b) and the insignificant correlation between the $\delta^{18}O$ and $\delta^{13}C$ data (Fig. 4c) indicate that the oxygen data of the selected layers pass the Hendy Test (Hendy, 1971). Another way to evaluate the isotopic equilibrium conditions is to use the Replication Test with contemporaneous stalagmite $\delta^{18}O$ records (Dorale and Liu, 2009). There was no significant difference between the contemporaneous $\delta^{18}O$ records of stalagmites LH4 and LH5 at the interval of 11.5–5.8 ka BP and for stalagmites LH5 and LH9 for 3.7–3.3 ka BP (Fig. 6). Evidence shows an insignificant kinetic effect on the $\delta^{18}O$ value, which is primarily of climatic origin.

Under isotopic equilibrium conditions, variations in stalagmite calcite $\delta^{18}O$ values are controlled by the drip water $\delta^{18}O$ composition and the cave temperature (Hendy, 1971). Early work by Shi et al. (1993) in northern China showed that the mean annual temperature during the Mid-Holocene was estimated to be 2–3 °C higher than the present and, therefore, only accounts for 25% of the changes in the Lianhua stalagmite $\delta^{18}O$ value (assuming −0.24‰/°C (O'Neil et al., 1969)). The fluctuations in stalagmite $\delta^{18}O$ values are dominated by the oxygen isotopic composition of the drip water. The "amount effect" dominates the precipitation $\delta^{18}O$ values in the Asian Monsoon regions (Araguás-Araguás et al., 1998; Yamanaka et al., 2004). Winter precipitation accounts for only 11% of the annual precipitation in Shanxi Province (Fig. 2). The Lianhua stalagmite $\delta^{18}O$ data mainly capture the summertime precipitation signature. By summarising these observations and performing model simulations, Liu et al. (2014) proposed that the stalagmite $\delta^{18}O$ records in northern China reflect the regional monsoon rainfall and represent the intensity of the EASM. On the basis of modern data, previous Chinese stalagmite studies, and simulations (Zhang et al., 2008; Cheng et al., 2009; Cai et al., 2010; Dong et al., 2010; Ma et al., 2012; D. Liu et al., 2013; Y. Liu et al., 2013), we interpreted the Lianhua Cave stalagmite $\delta^{18}O$ data as a qualitative proxy for regional precipitation and intensity of the EASM, with lower values indicating a stronger EASM and *vice versa*.

The composite Lianhua stalagmite $\delta^{18}O$ record, ranging from −7.3‰ to −11.4‰, is characterised by an enriched ^{18}O signal of 2.5‰ during the YD from 12.8 to 11.6 ka BP (Fig. 6). Before the YD, the $\delta^{18}O$ values gradually decreased from −9.0‰ to −10.0‰ during 14.5–12.8 ka BP. At the end of the YD, the $\delta^{18}O$ data show an abrupt decrease of ~3‰ at 11.6 ka BP. The subsequent $\delta^{18}O$ data continue to show highly depleted

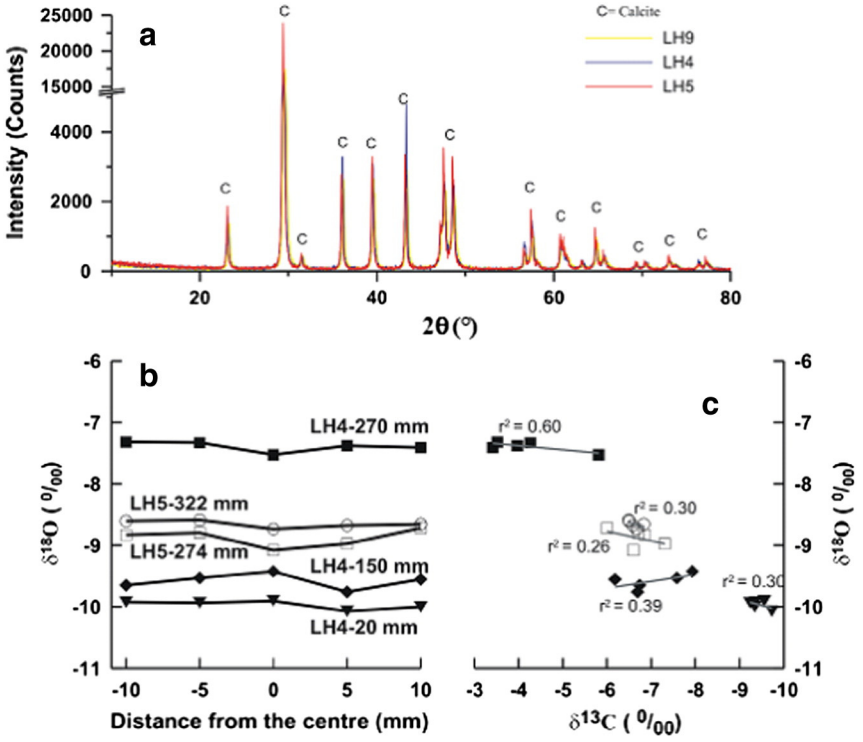

Fig. 4. **(a)** X-ray diffraction pattern and **(b)** Hendy Test (Hendy, 1971). The coeval $\delta^{18}O$ data show small changes of $2\sigma = \pm 0.06$–0.12‰ on five laminae of two stalagmites, LH4 and LH5. **(c)** The variable correlation and low correlation coefficient between $\delta^{18}O$ and $\delta^{13}C$ data denote an insignificant kinetic fractionation.

Table 1
Uranium and thorium isotopic compositions and ^{230}Th ages for stalagmites LH4, LH5, and LH9 by MC-ICP-MS.

Sample/	^{238}U	^{232}Th	$^{230}Th/^{232}Th$	$\delta^{234}U$	$^{230}Th/^{238}U$	Age (ka BP)	Age (ka BP)	$\delta^{234}U$
Depth (mm)	ppb	ppt	ppm[a]	Measured[b]	Activity[c]	Uncorrected	Corrected[c,d]	Initial[e]
LH4-10 mm	100.38 ± 0.15	2030.4 ± 8.7	120.1 ± 1.3	1660.3 ± 4.7	0.1471 ± 0.0015	6.117 ± 0.063	5.918 ± 0.118	1688.6 ± 4.8
LH4-38 mm	134.58 ± 0.35	3698 ± 16	95.5 ± 1.2	1660.0 ± 7.6	0.1589 ± 0.0019	6.625 ± 0.084	6.355 ± 0.159	1690.4 ± 7.7
LH4-53 mm	130.61 ± 0.47	2362 ± 11	155.7 ± 1.4	1714 ± 14	0.1706 ± 0.0015	6.983 ± 0.073	6.809 ± 0.113	1748 ± 14
LH4-93 mm	164.81 ± 0.44	1648.2 ± 7.2	287.5 ± 2.7	1717.2 ± 7.5	0.1741 ± 0.0015	7.124 ± 0.066	7.028 ± 0.082	1752.0 ± 7.7
LH4-138 mm	259.62 ± 0.86	2848 ± 13	297.8 ± 2.2	1714 ± 11	0.1979 ± 0.0013	8.145 ± 0.067	8.040 ± 0.085	1754 ± 11
LH4-145 mm	263.0 ± 1.7	2973 ± 12	300.8 ± 2.1	1768 ± 20	0.2034 ± 0.0018	8.211 ± 0.096	8.105 ± 0.109	1810 ± 20
LH4-156 mm	283.52 ± 0.63	627.7 ± 6.0	1526 ± 16	1726.0 ± 7.5	0.2052 ± 0.0010	8.420 ± 0.050	8.399 ± 0.051	1767.7 ± 7.6
LH4-166 mm	329.10 ± 0.71	1955.6 ± 8.1	589.9 ± 4.2	1713.1 ± 6.9	0.2123 ± 0.0013	8.766 ± 0.060	8.709 ± 0.067	1756.1 ± 7.1
LH4-181 mm	328.42 ± 0.26	7345 ± 29	166.4 ± 1.4	1699.9 ± 3.0	0.2254 ± 0.0017	9.378 ± 0.072	9.162 ± 0.130	1744.8 ± 3.1
LH4-213 mm	360.54 ± 0.98	1022.6 ± 8.2	1346 ± 11	1637.3 ± 8.9	0.23128 ± 0.00089	9.872 ± 0.053	9.844 ± 0.054	1683.8 ± 9.2
LH4-234 mm	796.61 ± 0.65	395.9 ± 5.1	8485 ± 111	1567.9 ± 3.1	0.25538 ± 0.00051	11.263 ± 0.027	11.257 ± 0.028	1618.9 ± 3.2
LH4-265 mm	799.89 ± 0.90	172.0 ± 5.9	20629 ± 704	1547.8 ± 3.9	0.26873 ± 0.00061	11.981 ± 0.035	11.978 ± 0.035	1601.4 ± 4.1
LH4-276 mm	759.81 ± 0.64	151.5 ± 5.5	22751 ± 826	1533.7 ± 3.4	0.27410 ± 0.00071	12.305 ± 0.038	12.303 ± 0.038	1588.2 ± 3.5
LH4-284 mm	819.41 ± 0.75	222.4 ± 4.6	17278 ± 355	1551.3 ± 3.9	0.28400 ± 0.00044	12.680 ± 0.029	12.677 ± 0.029	1608.2 ± 4.0
LH4-330 mm	872.0 ± 1.3	293.6 ± 6.5	15611 ± 345	1503.3 ± 5.1	0.31832 ± 0.00070	14.597 ± 0.047	14.594 ± 0.047	1566.9 ± 5.3
LH5-14 mm	143.26 ± 0.70	2043.5 ± 8.1	101.57 ± 0.83	1713 ± 12	0.08771 ± 0.00076	3.514 ± 0.035	3.376 ± 0.077	1730 ± 12
LH5-54 mm	139.51 ± 0.51	883.6 ± 5.8	252.0 ± 2.2	1771.4 ± 8.7	0.09667 ± 0.00066	3.801 ± 0.029	3.741 ± 0.032	1790.5 ± 8.8
LH5-62 mm	121.36 ± 0.43	8363 ± 33	32.98 ± 0.47	1689.3 ± 8.3	0.1376 ± 0.0020	5.645 ± 0.085	4.971 ± 0.348	1713.5 ± 8.6
LH5-148 mm	111.05 ± 0.30	2058.0 ± 7.9	148.1 ± 1.2	1655.0 ± 7.2	0.1662 ± 0.0013	6.952 ± 0.058	6.770 ± 0.108	1687.3 ± 7.4
LH5-161 mm	353.88 ± 0.98	657.6 ± 5.9	1854.7 ± 17	1676.4 ± 8.5	0.20843 ± 0.00078	8.723 ± 0.044	8.705 ± 0.045	1718.4 ± 8.7
LH5-181 mm	313.12 ± 0.31	3580 ± 11	326.7 ± 2.0	1683.5 ± 3.1	0.2262 ± 0.0013	9.474 ± 0.056	9.363 ± 0.079	1728.9 ± 3.2
LH5-230 mm	408.45 ± 0.41	459 ± 27	3057 ± 205	1680.7 ± 3.1	0.23891 ± 0.00059	10.039 ± 0.029	10.028 ± 0.029	1729.3 ± 3.2
LH5-377 mm	734.5 ± 1.8	451.4 ± 5.7	7074 ± 91	1565.8 ± 7.5	0.26329 ± 0.00081	11.639 ± 0.052	11.633 ± 0.052	1618.5 ± 7.8
LH9-7 mm	143.22 ± 0.23	570.5 ± 9.3	241.3 ± 3.9	2705.3 ± 7.4	0.05171 ± 0.00040	1.472 ± 0.012	1.444 ± 0.019	2716.9 ± 7.4
LH9-28 mm	124.79 ± 0.18	381.5 ± 3.5	314.1 ± 3.5	2084.7 ± 5.1	0.05816 ± 0.00038	2.014 ± 0.014	1.988 ± 0.019	2096.5 ± 5.2
LH9-58 mm	99.0 ± 4.8	3210.2 ± 8.8	79.2 ± 1.1	4249 ± 287	0.1555 ± 0.0079	3.211 ± 0.248	3.048 ± 0.249	4287 ± 289
LH9-102 mm	115.68 ± 0.15	3210 ± 12	98.2 ± 1.3	3148.0 ± 6.5	0.1650 ± 0.0021	4.352 ± 0.056	4.176 ± 0.104	3185.9 ± 6.6

Analytical errors are 2σ of the mean.

[a] The degree of detrital ^{230}Th contamination is indicated by the $^{230}Th/^{232}Th$ atomic ratio instead of the activity ratio.

[b] $\delta^{234}U = ([^{234}U/^{238}U]_{activity} - 1) \times 1000$.

[c] $[^{230}Th/^{238}U]_{activity} = 1 - e^{-\lambda 230 T} + (\delta^{234}U_{measured}/1000)[\lambda_{230}/(\lambda_{230} - \lambda_{234})](1 - e^{-(\lambda 230 - \lambda 234) T})$, where T is the age. Decay constants are 9.1577×10^{-6} year^{-1} for ^{230}Th, 2.8263×10^{-6} year^{-1} for ^{234}U and 1.55125×10^{-6} year^{-1} for ^{238}U (Cheng et al., 2000).

[d] Age (before 1950 CE) corrections were made using a $^{230}Th/^{232}Th$ atomic ratio of 4 ± 2 ppm, which is value for material at secular equilibrium with the crustal $^{232}Th/^{238}U$ value of 3.8 and arbitrarily assumed uncertainty of 50%.

[e] $\delta^{234}U$ corrected was calculated based on ^{230}Th age (T), i.e., $\delta^{234}U_{initial} = \delta^{234}U_{measured}$ x $e^{\lambda 234 * T}$, T is corrected age.

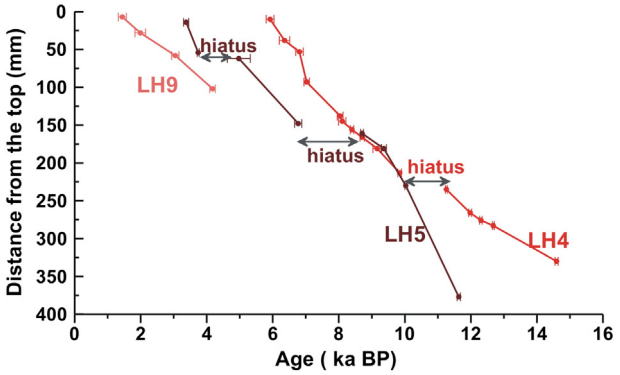

Fig. 5. Plot of the age models for three Lianhua stalagmites, LH4, LH5, and LH9. All ages with a 2σ error are reported as thousand years before present (ka BP, before 1950 CE).

values of −11‰ to −10‰ until ~6 ka BP, and then show an increasing trend of 2–3‰ from the Mid- to Late Holocene. One prominent abrupt isotopic anomaly, with an amplitude of >1‰ that lasted >100 years during the Holocene, was distinguished at ~8.2 ka BP.

5. Discussion

5.1. Comparison of records from the Lianhua and other caves

To obtain an in-depth understanding of the change in climate during the Holocene across China, we compared our records with previous and precisely dated speleothem records from the following caves: Qunf (Fleitmann et al., 2003), Dongge (Dykoski et al., 2005), Heshang (Hu et al., 2008), Sanbao (Wang et al., 2005; Dong et al., 2010), and Jiuxian (Cai et al., 2010). These caves cover a large region from 17°N to 38°N (Fig. 7). All comparable stalagmite $\delta^{18}O$ profiles track the summer insolation. For example, during the interval between the Early and Mid-Holocene at 11.6–6 ka BP, a prolonged period of strong EASM precipitation is expressed in all cave records, pacing the high-insolation conditions (Fig. 7). The similarity is reflected by the high correlation coefficients between Lianhua and other caves over the past 14.5 ka BP: r = 0.79 (n = 232, p = 0.05) for Lianhua/Sanbao, 0.72 (n = 267, p = 0.05) for Lianhua/Dongge, and 0.72 (n = 188, p = 0.05) for Lianhua/Qunf.

The Lianhua $\delta^{18}O$ record shows that the intensity of the EASM decreased at 12.8 ka BP, the end of the Bølling–Allerød period, and abruptly increased at 11.6 ka BP, matching the transient timing and duration of the YD recorded in the caves of southern and central China (Fig. 7), influenced by both the India Summer Monsoon (ISM) and the EASM, and also shown by Moomi Cave, Socotra Island, Yemen (Shakun et al.,

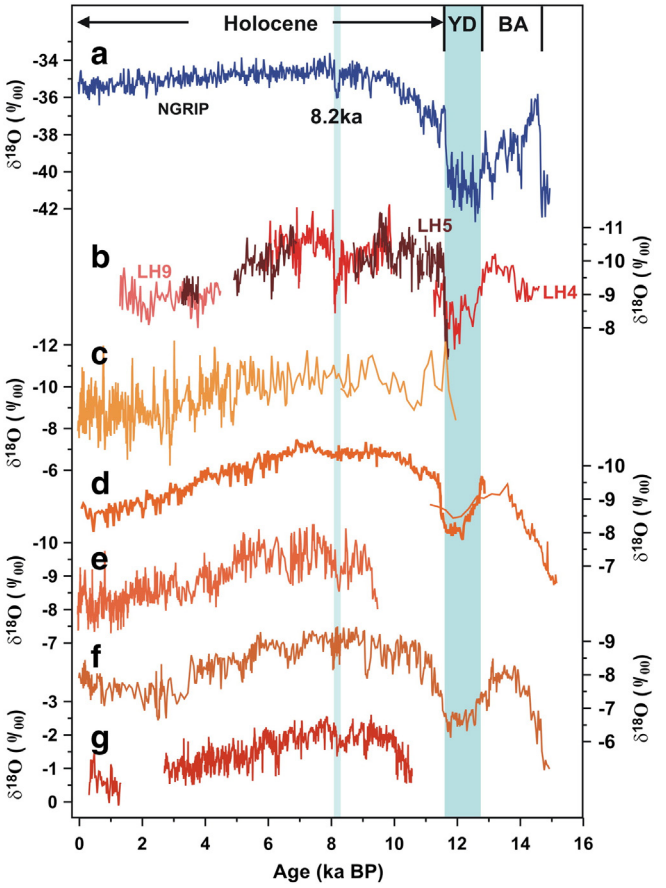

Fig. 7. The $\delta^{18}O$ time series of **(a)** Greenland NGRIP ice core (relative to Vienna Standard Mean Ocean Water (VSMOW); Vinther et al., 2006) and stalagmites from caves at: **(b)** Lianhua (this study) in northern China, **(c)** Jiuxian (Cai et al., 2010), **(d)** Sanbao (Wang et al., 2008; Dong et al., 2010), **(e)** Heshang (Hu et al., 2008) in central China, **(f)** Dongge (Dykoski et al., 2005) in south-western China, and **(g)** Qunf (Fleitmann et al., 2003) in southern Oman. All the sequences feature concurrent periods, such as Bølling–Allerød (BA), Younger Dryas (YD), and the 8.2-ka event (8.2 ka) over the last deglaciation.

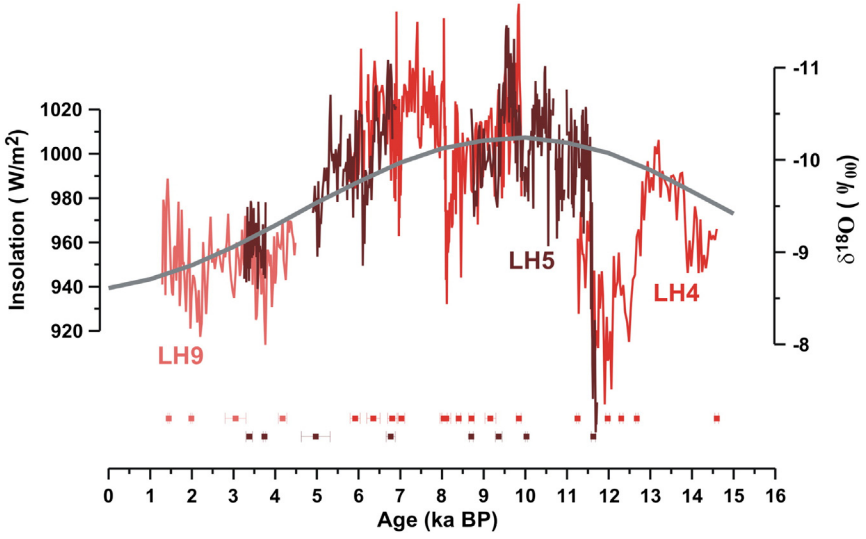

Fig. 6. The $\delta^{18}O$ time series of stalagmites LH4 (red), LH5 (dark red), and LH9 (pink). The ^{230}Th ages with a 2σ uncertainty are colour-coded by stalagmite. The grey line denotes a mid-July solar insolation at 30°N (Berger, 1978).

2007), in the ISM region. A prominently abrupt 150-year weak monsoon interval at 8.2 ka BP was observed in Lianhua Cave, concurrent with the low-precipitation conditions recorded in the Heshang, Dongge, and Qunf caves (Fig. 7).

The consistency of the stalagmite proxy records from the remote locations shown in Fig. 7 indicates synchronous hydrological dynamics on a millennial-orbital timescale in the ASM region, as well as in China. Our Lianhua record supports the view that insolation is the primary factor controlling regional hydrological variations in the ASM realm (Wang et al., 2005; Cai et al., 2010; Dong et al., 2010). This result is attributed to the large-scale monsoon circulation field and the high correlation of precipitation $\delta^{18}O$ between eastern China and the upstream Indian Ocean region (Liu et al., 2014). Modern observations show that in summer, the warm Indian Ocean can increase the ISM precipitation and enhance the transport of moisture, leading the moisture front deep into China (Guo and Wang, 1998). Latent heating related to monsoon rainfall further intensifies the circulation of the EASM over eastern China (Webster et al., 1998), where the Meiyu front interacts with westerly jets coming down from the mid and high latitudes, leading to frequent and heavy rainfall (Chiang et al., 2015).

5.2. Weak ASM conditions during the YD, 8.2-ka BP, and 4.2-ka BP events

It has been proposed that a millennial-scale weak ASM with low summer precipitation in East Asia during the YD was induced by a pronounced input of meltwater into the North Atlantic (*e.g.*, Wang et al., 2001; McManus et al., 2004; Denton et al., 2010). A slow-down of the Atlantic meridional overturning circulation (AMOC) may have resulted in a high-latitude cooling in the northern hemisphere (NH), as recorded in the Greenland ice cores (Fig. 7a). It could have triggered a southward shift of the inter-tropical convergence zone (Wang et al., 2004), as well as a weakening of the ASM with low precipitation values. Thus, the resulting synchronous aridity would have prevailed over the entire ASM region (Fig. 7; Fig. 1 of Liu et al., 2014).

Recent work on stalagmites in central and northern China (Ma et al., 2012; D. Liu et al., 2013) shows that the full transition from the end of the YD to the Early Holocene was <20 years, according to layer-counted $\delta^{18}O$ records. Although stalagmite laminae do not always deposit annually, as suggested by Shen et al. (2013), a rapid decrease of ~3‰ in the Lianhua $\delta^{18}O$ data within 80 years at the onset of the Early Holocene supports that EASM conditions resumed on a decadal timescale. However, it is notable that the absolute amplitude of stalagmite $\delta^{18}O$ enrichment at the YD is 2–2.5‰ in the Lianhua and Kulishu caves, 0.5–1‰ higher than the 1–1.5‰ enrichment in the Sanbao and Qingtian caves, and the 1.5–2‰ enrichment in the Dongge and Yamen caves (Fig. 3 of D. Liu et al., 2013). This suggests that the drought in northern China was more severe than in other regions and that there was a variation in the heterogeneous precipitation over the entire monsoonal region of China. This stalagmite $\delta^{18}O$ enrichment is less pronounced in the Moomi Cave in Yemen in the tropical ISM region (Shakun et al., 2007). The different meridional hydroclimatic responses in the ASM region may be attributable to NH high-latitude forcing originating from the North Atlantic (*e.g.*, Shakun and Carlson, 2010).

The 8.2-ka BP event is regarded as being the most remarkable cooling episode during the Holocene that is registered in the Greenland ice core records (Fig. 7a) and was first highlighted by Alley et al. in 1997. Similar to the initialisation of the YD, this event was triggered by a massive influx of fresh water into the North Atlantic, resulting in a slowdown of the AMOC, a rapid cooling of the North Atlantic, and a subsequent change in climate in low-latitude regions (*e.g.*, Barber et al., 1999; Denton et al., 2010). An induced synchronous centennial-scale drought occurred over the entire ASM region (Fig. 8). However, the regions apparently experienced different arid conditions. The reducing trend in stalagmite ^{18}O enrichment (from ~1.7‰ in Lianhua Cave in northern China and ~1.5‰ in Heshang Cave in central China to ~0.8‰ in Dongge Cave in southwestern China (Fig. 8)) suggests that this aridity

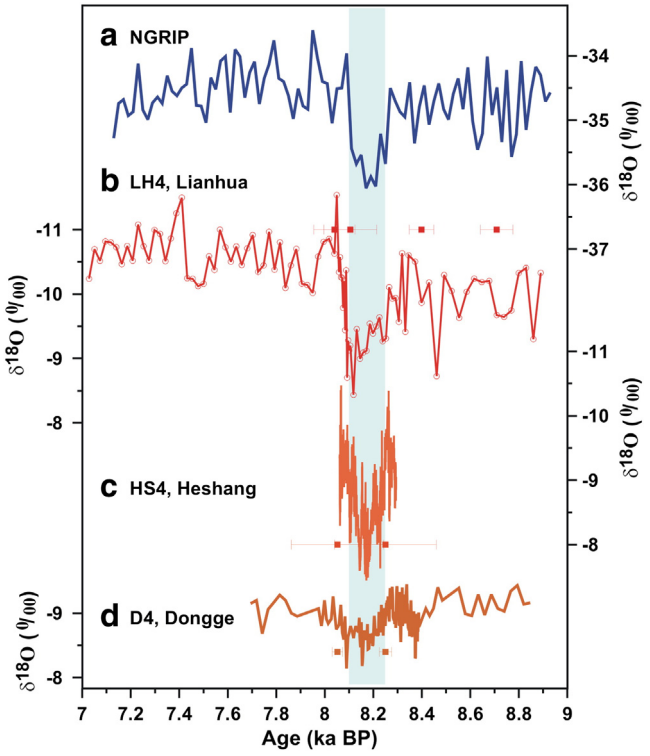

Fig. 8. The $\delta^{18}O$ time series during 9–7 ka BP of **(a)** Greenland NGRIP ice core (relative to VSMOW; Vinther et al., 2006) and stalagmites **(b)** LH4 from Lianhua (this study), **(c)** HS4 from Heshang (Hu et al., 2008), and **(d)** D4 from Dongge (Dykoski et al., 2005). The ^{230}Th ages with a 2σ uncertainty are colour-coded by stalagmite. The shaded band represents the period of the 8.2-ka event.

was relieved moving southward. The largest amplitude shown in the Lianhua $\delta^{18}O$ record also suggests that hydroclimatic perturbation in northern China is very sensitive to this NH high-latitude forcing. Recent work at Nuanhe Cave (41°20′N, 124°55′E, Wu et al., 2012), located in the Liaoning Province in northeastern China, suggests that changes in stalagmite $\delta^{13}C$ and Ba/Ca proxy records indicate that the local environment responded to strong winter monsoon conditions resulting from NH high-latitude forcing. However, the faintness in the $\delta^{18}O$ record implies that summer precipitation did not decrease markedly (Wu et al., 2012). More contrasting local proxy data are needed to clarify this site-specific muted response.

The drought period occurring at ~4.2 ka BP, called "Bond Event 3" (Bond et al., 1997), is not registered in the Greenland ice cores but is clearly recorded in the North Atlantic and also in NH regions (Fig. 2 of deMenocal, 2001). This event possibly caused the collapse of ancient Eurasian civilisations (deMenocal, 2001; Wu and Liu, 2004 and reference therein) and could induce a weak summer monsoon condition, which is registered in the stalagmites of some Chinese caves: for example, in Dongge Cave in southwestern China (Wang et al., 2005) and Heshang Cave in central China (Hu et al., 2008). However, it is not noticeable in Shigao Cave in southwestern China (Jiang et al., 2012), Sanbao Cave in central China (Dong et al., 2010), or Lianhua Cave in northern China (this study). The changeable climatic responses imply a weak influence of this high-latitude forcing on the entire mainland.

5.3. Comparison of the different proxy records in northern China

The palaeo-hydroclimatic heterogeneity between different natural archives in northern China and other regions in the ASM realm has been debated for decades. For example, the proxy sequences of the Jingbian desert/loess deposits (37°40–50′N, 109°10–20′E; Xiao et al., 2002) and the Daihai Lake sediments (40°29–37′N, 112°33–46′E; Xiao et al., 2004) (refer to Fig. 1b for site locations) show that summer

monsoonal precipitation was generally weak in the Early Holocene and was stronger during the Mid-Holocene. However, studies of swamp sediments at Yanhaizi (40°06–10′N, 108°25–29′E; Chen et al., 2003) and Zheyeze (39°00′N, 103°20′E; Chen et al., 2006) in western China suggest a reverse trend, in which monsoonal precipitation was enhanced in the Early Holocene and weakened in the Mid-Holocene. A study of the loess magnetic susceptibility at Baxie (35°33′N, 103°35′E) suggested a strong EASM during the YD (An et al., 1993), which is inconsistent with the stalagmite records shown in Fig. 7. This weak EASM, with low summer precipitation during the YD, is also revealed in the magnetic susceptibility records (Fig. 9d) from the Baicaoyuan Section (Fig. 1b) but is not shown in the nearby (~50 km) Jingyuan Section in the western CLP (Sun et al., 2010; Zhao et al., 2013; Fig. 9d). The duration of a stable dune phase in the Mu Us Desert lasted from 8.8 to 5.6 ka BP (Lu et al., 2005; Sun et al., 2006), which is asynchronous with the high precipitation interval occurring at 11.6–6.0 ka BP in the Lianhua stalagmites (Fig. 9a and e). To clarify this debate, we compared the Lianhua stalagmite record with previously published and well-dated proxy records from northern China (Fig. 9).

Using pollen data from Bayanchagan Lake (Fig. 1b), Jiang et al. (2006, 2009) quantitatively reconstructed changes in the Holocene EASM precipitation (Fig. 9b). The estimated summer monsoonal precipitation was as low as 300 mm/year on the CLP during the YD, increasing to 550 mm/year in the Early to Mid-Holocene, and then decreasing to 350 mm/year in the Late Holocene. A synthesised pollen-inferred semi-quantitative moisture index record (Zhao et al., 2009) features the same dynamics (Fig. 9c). Climate changes in both time series (Fig. 9b and c) are synchronous with those in the Lianhua record (Fig. 9a), within dating error. This consistency is also supported by recently synthesised carbonate oxygen isotope records from ten Chinese lakes within the monsoon region, exhibiting more negative values linked to strong EASM precipitation in the first half of the Holocene (Zhang et al., 2011). We argue that these discrepancies between the reconstructed palaeoclimate sequences of proxy records, as stated in the previous paragraph, are principally attributable to (1) low-resolution (centennial-to-multi-centennial) records with an absence of robust age models, and (2) the complexity and fidelity of natural archives.

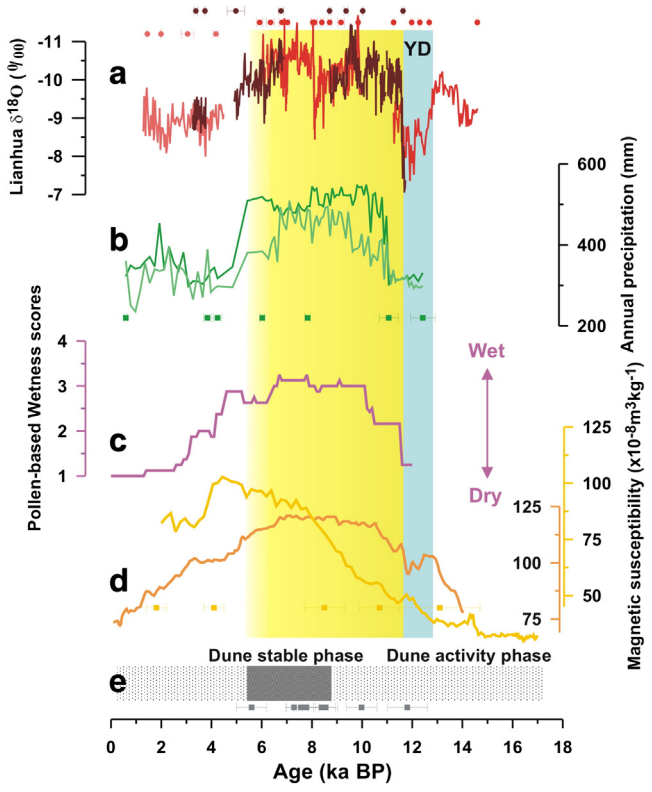

Fig. 9. Different proxy records in the CLP. **(a)** Lianhua stalagmite $\delta^{18}O$ (this study). **(b)** Pollen-inferred annual precipitation in Bayanchagan Lake (Jiang et al., 2006, 2009). **(c)** Relative moisture index inferred from fossil pollen data (Zhao et al., 2009). **(d)** Magnetic susceptibility of the Baicaoyuan (orange; Zhao et al., 2013) and Jingyuan sections (dark yellow; Sun et al., 2010, 2012) (refer to Fig. 1 for site locations) with the age models constructed from the grain size and magnetic susceptibility (Fig. 4 of Zhao et al., 2013). **(e)** Stratigraphic evidence of dune phases in the Mu Us Desert (Lu et al., 2005; Sun et al., 2006; Mason et al., 2009). The yellow bar denotes a stalagmite-inferred strong early-Holocene EASM interval between 11.6 and ~6.0 ka BP. Ages with a 2σ uncertainty are colour-coded by record.

6. Conclusions

Absolute-dated stalagmite records from Lianhua Cave reveal a detailed history of the EASM in northern China since the last deglaciation period. The concurrency of stalagmite $\delta^{18}O$ sequences along a latitudinal transect from 17°N to 38°N suggests that millennial-orbital timescale hydrological dynamics are synchronous between northern China and other ASM regions. The enhanced values of 2.5‰ during the YD and 1.7‰ at the 8.2-ka BP event in the Lianhua Cave stalagmite ^{18}O records, when compared to others in the ASM region, imply different meridional responses to weak precipitation conditions throughout the ASM region. The heterogeneity of proxy-inferred hydroclimatic sequences in northern China is most likely attributable to the complexity of formation and/or chronological uncertainty in the natural archives.

Acknowledgments

Authors thank W. Zhang, S. Wu, and J.L. Li for fieldwork, including sample collecting, and C. Deng and Z.Q. Zhang for assistance with stable isotope measurement. Thanks are also given to two anonymous reviewers for his/her critical and instructive comments. This work was supported by grants from the National Nature Science Foundation of China (Nos. 41102216, 41472317 to Dong, J.G., 41172314 to Kong, X.G., and 41372189 to Jang, X.Y.), the Open Foundations of the State Key Laboratory of Loess and Quaternary Geology, Institute of Earth Environment, CAS, China (No. SKLLQG1211 to Dong, J.G.), and the Jiangsu Key Laboratory of Environmental Change and Ecological Construction. We also thank Taiwan ROC MOST (102-2116-M-002-016, 103-2119-M-002-022) and the National Taiwan University (101R7625) for their financial support.

References

Alley, R.B., Mayewski, P.A., Sowers, T., Stuiver, M., Taylor, K.C., Clark, P.U., 1997. Holocene climatic instability: a prominent widespread event 8200 years ago. Geology 25, 483–486.
An, Z.S., Porter, S.C., Zhou, W.J., Lu, Y.C., Donahue, D.J., Head, M.J., Wu, X.H., Ren, J.Z., Zheng, H.B., 1993. Episode of strengthened summer monsoon climate of Younger Dryas age on the loess plateau of central China. Quat. Res. 39, 45–54.
Araguás-Araguás, L., Froehlich, K., Rozanski, K., 1998. Stable isotope composition of precipitation over southeast Asia. J. Geophys. Res. 103, 28721–28742.
Barber, D.C., Dyke, A., Hillaire-Marcel, C., Jennings, A.E., Andrews, J.T., Kerwin, M.W., Bilodeau, G., McNeely, R., Southon, J., Morehead, M.D., Gagnon, J.M., 1999. Forcing of the cold event of 8,200 years ago by catastrophic drainage of Laurentide lakes. Nature 400, 344–348.
Berger, A.L., 1978. Long-term variations of caloric insolation resulting from the Earth's orbital elements. Quat. Res. 9, 139–167.
Bond, G., Showers, W., Cheseby, M., Lotti, R., Almasi, P., deMenocal, P., Priore, P., Cullen, H., Hajdas, I., Bonani, G., 1997. A pervasive millennial-scale cycle in North Atlantic. Science 278, 1257–1266.
Cai, Y., Tan, L., Cheng, H., An, Z., Edwards, R.L., Kelly, M.J., Kong, X., Wang, X., 2010. The variation of summer monsoon precipitation in central China since the last deglaciation. Earth Planet. Sci. Lett. 291, 21–31.
Cai, Y.J., Fung, I.Y., Edwards, R.L., An, Z.S., Cheng, H., Lee, J.-E., Tan, L.C., Shen, C.-C., Wang, X.F., Day, J.A., Zhou, W.J., Kelly, M.J., Chiang, J.C.H., 2015. Variability of stalagmite-inferred Indian monsoon precipitation over the past 252,000 y. Proc. Natl. Acad. Sci. U. S. A. 112, 2954–2959.
Chen, F.H., Zhu, Y., Li, J.J., Shi, Q., Jin, L.Y., Wünnemann, B., 2001. Abrupt Holocene changes of the Asian monsoon at millennial- and centennial-scales: evidence from lake sediment document in Minqin Basin, NW China. Chin. Sci. Bull. 46, 1942–1947.
Chen, C.-T.A., Lan, H.C., Lou, J.Y., Chen, Y.C., 2003. The dry Holocene Megathermal in Inner Mongolia. Palaeogeogr. Palaeoclimatol. Palaeoecol. 193, 181–200.

Chen, F.H., Cheng, B., Zhao, Y., Zhu, Y., Madsen, D., 2006. Holocene environmental change inferred from a high-resolution pollen record, Lake Zhuyeze, arid China. The Holocene 16, 657–684.
Cheng, H., Edwards, R.L., Hoff, J., Gallup, C.D., Richards, D.A., Asmerom, Y., 2000. The half-lives of uranium-234 and thorium-230. Chem. Geol. 169, 17–33.
Cheng, H., Fleitmann, D., Edwards, R.L., Wang, X.F., Cruz, W.F., Auler, A.S., Mangini, A., Wang, Y.J., Kong, X.G., Burns, S., Matter, A., 2009. Timing and structure of the 8.2 kyr B.P. event inferred from $\delta^{18}O$ records of stalagmites from China, Oman, and Brazil. Geology 37, 1007–1010.
Cheng, H., Edwards, R.L., Shen, C.-C., Polyak, V.J., Asmerom, Y., Woodhead, J., Hellstrom, J., Wang, Y.J., Kong, X.G., Spötl, C., Wang, X.F., Alexander, E.C., 2013. Improvements in ^{230}Th dating, ^{230}Th and ^{234}U half-life values, and U-Th isotopic measurements by multi-collector inductively coupled plasma mass spectrometry. Earth Planet. Sci. Lett. 372, 82–91.
Chiang, J.C.H., Fung, I., Wu, C.-H., Cai, Y.J., Edman, J.P., Liu, Y.W., Day, J.A., Bhattacharya, T., Mondal, Y., 2015. Role of seasonal transitions and westerly jets in East Asian plaeoclimate. Quat. Sci. Rev. 108, 111–129.
deMenocal, P.B., 2001. Cultural responses to climate change during the Late Holocene. Science 292, 667–673.
Denton, G.H., Anderson, R.F., Toggweiler, J.R., Edwards, R.L., Schaefer, J.M., Putnam, A.E., 2010. The last glacial termination. Science 328, 1652–1656.
Dong, J.G., Wang, Y.J., Cheng, H., Hardt, B., Edwards, R.L., Kong, X.G., Wu, J.Y., Chen, S.T., Liu, D.B., Jiang, X.Y., Zhao, K., 2010. A high-resolution stalagmite record of the Holocene East Asian monsoon from Mt Shennongjia, central China. The Holocene 20, 257–264.
Dorale, J., Liu, Z.H., 2009. Limitations of Hendy Test criteria in judging the paleoclimatic suitability of speleothems and the need for replication. J. Cave Karst Stud. 71, 73–80.
Dykoski, C.A., Edwards, R.L., Cheng, H., Yuan, D., Cai, Y., Zhang, M., Lin, Y., Qing, J., An, Z., Revenaugh, J., 2005. A high-resolution, absolute-dated Holocene and deglacial Asian monsoon record from Dongge Cave, China. Earth Planet. Sci. Lett. 233, 71–86.
Fleitmann, D., Burns, S.J., Mudelsee, M., Neff, U., Kramers, J., Mangini, A., Matter, A., 2003. Holocene forcing of the Indian monsoon recorded in a stalagmite from Southern Oman. Science 300, 1737–1739.
Guo, Q., Wang, J., 1998. A comparison of the summer precipitation in India with that in China. J. Trop. Meteorol. 4, 53–60 (in Chinese).
Hendy, C.H., 1971. The isotopic geochemistry of speleothems-I. The calculation of the effects of different modes of formation on the isotopic composition of speleothems and their applicability as palaeoclimatic indicators. Geochim. Cosmochim. Acta 35, 801–824.
Hong, Y.T., Hong, B., Lin, Q.H., Shibata, Y., Hirota, M., Zhu, Y.X., Leng, X.T., Wang, Y., Wang, H., Yi, L., 2005. Inverse phase oscillations between the East Asian and Indian Ocean summer monsoons during the last 12000 years and paleo-El Niño. Earth Planet. Sci. Lett. 231, 337–346.
Hong, B., Hong, Y.T., Lin, Q.H., Shibata, Y., Uchida, M., Zhu, Y.X., Leng, X.T., Wang, Y., Cai, C.C., 2010. Anti-phase oscillation of Asian monsoons during the Younger Dryas period: evidence from peat cellulose $\delta^{13}C$ of Hani, Northeast China. Palaeogeogr. Palaeoclimatol. Palaeoecol. 297, 214–222.
Hu, C.Y., Henderson, G.M., Huang, J., Xie, S., Sun, Y., Johnson, K.R., 2008. Quantification of Holocene Asian monsoon rainfall from spatially separated cave records. Earth Planet. Sci. Lett. 266, 221–232.
Jiang, W.Y., Guo, Z.T., Sun, X.J., Wu, H.B., Chu, G.Q., Yuan, B.Y., Hatté, C., Guiot, J., 2006. Reconstruction of climate and vegetation changes of Lake Bayanchagan (Inner Mongolia): Holocene variability of the East Asian monsoon. Quat. Res. 65, 411–420.
Jiang, W.Y., Guiot, J., Chu, G., Wu, H.B., Yuan, B.Y., Hatté, C., Guo, Z.T., 2009. An improved methodology of the modern analogues technique for palaeoclimate reconstruction in arid and semi-arid regions. Boreas 39, 145–153.
Jiang, X.Y., He, Y.Q., Shen, C.C., Kong, X.G., Li, Z.Z., Chang, Y.W., 2012. Stalagmite-inferred Holocene precipitation in northern Guizhou Province, China, and asynchronous termination of the climatic optimum in the Asian monsoon territory. Chin. Sci. Bull. 57, 795–801.
Jin, Z., Wu, J., Cao, J., Wang, S., Shen, J., Gao, N., Zou, C., 2004. Holocene chemical weathering and climatic oscillations in north China: evidence from lacustrine sediments. Boreas 33, 260–266.
Li, X.Q., Zhou, J., Shen, J., Weng, C.Y., Zhao, H.L., Sun, Q.L., 2004. Vegetation history and climatic variations during the last 14 ka BP inferred from a pollen record at Daihai Lake, north-central China. Rev. Palaeobot. Palynol. 132, 195–205.
Li, X.Q., Shang, X., Dodson, J., Zhou, X.Y., 2009. Holocene agriculture in the Guanzhong Basin in NW China indicated by pollen and charcoal evidence. The Holocene 19, 1213–1220.
Liu, T.S., Ding, Z.L., 1998. Chinese loess and the paleomonsoon. Annu. Rev. Earth Planet. Sci. 26, 111–145.
Liu, D.B., Wang, Y.J., Cheng, H., Kong, X.G., Chen, S.T., 2013. Centennial-scale Asian monsoon variability during the mid-Younger Dryas from Qingtian Cave, central China. Quat. Res. 80, 199–206.
Liu, Y.H., Henderson, G.M., Hu, C.Y., Mason, A.J., Charnley, N., Johnson, K.R., Xie, S.C., 2013. Links between the East Asian monsoon and North Atlantic climate during the 8,200 year event. Nat. Geosci. 6, 117–120.
Liu, Z.Y., Wen, X.Y., Brady, E.C., Otto-Bliesner, B., Yu, G., Lu, H.Y., Cheng, H., Wang, Y.J., Zheng, W.P., Ding, Y.H., Edwards, R.L., Cheng, J., Liu, W., Yang, H., 2014. Chinese cave records and the East Asia Summer Monsoon. Quat. Sci. Rev. 83, 115–128.
Lone, M.A., Ahmad, S.M., Dung, N.C., Shen, C.-C., Raza, W., Kumar, A., 2014. Speleothem based 1,000-year high resolution record of Indian monsoon variability during the last deglaciation. Palaeogeogr. Palaeoclimatol. Palaeoecol. 395, 1–8.
Lu, H.Y., Miao, X.D., Zhou, Y.L., Mason, J., Swinehart, J., Zhang, J.F., Zhou, L.P., Yi, S.W., 2005. Late Quaternary aeolian activity in the Mu Us and Otindag dune fields (north China) and lagged response to insolation forcing. Geophys. Res. Lett. 32, L21716. http://dx.doi.org/10.1029/2005GL024560.
Lu, H.Y., Yi, S.W., Liu, Z.Y., Mason, J.A., Jiang, D.B., Cheng, J., Steven, T., Xu, Z.W., Zhang, E.L., Jin, L.Y., Zhang, Z.H., Guo, Z.T., Wang, Y., Otto-Bliesner, B., 2013. Variation of East Asian monsoon precipitation during the past 21 k.y. and potential CO2 forcing. Geology 41, 1023–1026.
Ma, Z.B., Cheng, H., Tan, M., Edwards, R.L., Li, H.C., You, C.F., Duan, W.H., Wang, X., Kelly, M.J., 2012. Timing and structure of the Younger Dryas event in northern China. Quat. Sci. Rev. 41, 83–93.
Mason, J.A., Lu, H., Zhou, Y., Miao, X., Swinehart, J.B., Liu, Z., Goble, R.J., Yi, S., 2009. Dune mobility and aridity at the desert margin of northern China at a time of peak monsoon strength. Geology 37, 947–950.
McManus, J.F., Francois, R., Gherardi, J.-M., Keigwin, L.D., Brown-Leger, S., 2004. Collapse and rapid resumption of Atlantic meridional circulation linked to deglacial climate changes. Nature 428, 834–837.
O'Neil, J.R., Clayton, R.N., Mayeda, T.K., 1969. Oxygen isotope fractionation in divalent metal carbonates. J. Chem. Phys. 51, 5547–5558.
Qian, X.P., 1960. Development of the Carbonate Karst, in Shanxi plateau. Hydrogeol. Eng. Geol. 4, 19–23 (in Chinese).
Shakun, J.D., Carlson, A.E., 2010. A global perspective on Last Glacial Maximum to Holocene climate change. Quat. Sci. Rev. 29, 1801–1816.
Shakun, J.D., Burn, S.J., Fleitmann, D., Kramers, J., Matter, A., Al-Subbary, A., 2007. A high-resolution, absolute-dated deglacial speleothem record of Indian Ocean climate from Socotra Island, Yemen. Earth Planet. Sci. Lett. 259, 442–456.
Shen, C.-C., Lawrence Edwards, R., Cheng, H., Dorale, J.A., Thomas, R.B., Bradley Moran, S., Weinstein, S.E., Edmonds, H.N., 2002. Uranium and thorium isotopic and concentration measurements by magnetic sector inductively coupled plasma mass spectrometry. Chem. Geol. 185, 165–178.
Shen, C.-C., Cheng, H., Edwards, R.L., Moran, S.B., Edmonds, H.N., Hoff, J.A., Thomas, R.B., 2003. Measurement of attogram quantities of ^{231}Pa in dissolved and particulate fractions of seawater by isotope dilution thermal ionization mass spectroscopy. Anal. Chem. 75, 1075–1079.
Shen, J., Liu, X.Q., Wang, S.M., Matsumoto, R., 2005. Palaeoclimatic changes in the Qinghai Lake area during the last 18,000 years. Quat. Int. 136, 131–140.
Shen, C.-C., Wu, C.-C., Cheng, H., Edwards, R.L., Hsieh, Y.-T., Gallet, S., Chang, C.-C., Li, T.-Y., Lam, D.D., Kano, A., Hori, M., Spotl, C., 2012. High-precision and high-resolution carbonate ^{230}Th dating by MC-ICP-MS with SEM protocols. Geochim. Cosmochim. Acta 99, 71–86.
Shen, C.-C., Lin, K., Duan, W.H., Jiang, X.Y., Partin, J.W., Edwards, R.L., Cheng, H., Tan, M., 2013. Testing the annual nature of speleothem banding. Sci. Rep. 3, 2633. http://dx.doi.org/10.1038/srep02633.
Shi, Y.F., Kong, Z.C., Wang, S.M., Tang, L.Y., Wang, F.C., Yao, T.D., Zhao, X.T., Zhang, P.Y., Shi, S.H., 1993. Mid-Holocene climates and environments in China. Glob. Planet. Chang. 7, 219–233.
Sinha, A., Cannariato, K.G., Stott, L.D., Li, H.C., You, C.F., Cheng, H., Edwards, R.L., Singh, I.B., 2005. Variability of southwest Indian summer monsoon precipitation during the Bølling–Allerød. Geology 33, 813–816.
Stebich, M., Mingram, J., Han, J.T., Liu, J.Q., 2009. Late Pleistocene spread of (cool-) temperate forests in Northeast China and climate changes synchronous with the North Atlantic region. Glob. Planet. Chang. 65, 56–70.
Stebich, M., Mingram, J., Moschen, R., Thiele, A., Schröder, C., 2010. Comments on "Anti-phase oscillation of Asian monsoons during the Younger Dryas period: Evidence from peat cellulose $\delta^{13}C$ of Hani, Northeast China" by B. Hong, Y.T. Hong, Q.H. Lin, Yasuyuki Shibata, Masao Uchida, Y.X. Zhu, X.T. Leng, Y. Wang and C.C. Cai [Palaeogeography, Palaeoclimatology, Palaeoecology 297 (2010) 214–222]. Palaeogeogr. Palaeoclimatol. Palaeoecol. 310, 464–470.
Sun, J.M., Li, S.H., Han, P., Chen, Y.Y., 2006. Holocene environmental changes in the central Inner Mongolia, based on single-aliquot-quartz optical dating and multi-proxy study of dune sands. Palaeogeogr. Palaeoclimatol. Palaeoecol. 233, 51–62.
Sun, Y.B., Wang, X.L., Liu, Q.S., Clemens, S.C., 2010. Impacts of post-depositional processes on rapid monsoon signals recorded by the last glacial loess deposits of northern China. Earth Planet. Sci. Lett. 289, 171–179.
Sun, Y.B., Clemens, S.C., Morrill, C., Lin, X.P., Wang, X.L., An, Z.S., 2012. Influence of Atlantic meridional overturning circulation on the East Asian winter monsoon. Nat. Geosci. 5, 46–49.
Vinther, B.M., Clausen, H.B., Johnsen, S.J., Rasmussen, S.O., Andersen, K.K., Buchardt, S.L., Dahl-Jensen, D., Seierstad, K., Siggaard-Andersen, M.-L., Steffensen, J.P., Svebssen, A., Olsen, J., Heinemeier, J., 2006. A synchronized dating of three Greenland ice cores throughout the Holocene. J. Geophys. Res. 111, D13102. http://dx.doi.org/10.1029/2005JD006921.
Wang, Y.J., Cheng, H., Edwards, R.L., An, Z.S., Wu, J.Y., Shen, C.-C., Dorale, J.A., 2001. A high-resolution absolute-dated Late Pleistocene monsoon record from Hulu Cave, China. Science 294, 2345–2348.
Wang, X.F., Auler, A.S., Edwards, R.L., Cheng, H., Cristalli, P.S., Smart, P.L., Richards, D.A., Shen, C.-C., 2004. Wet periods in northeastern Brazil over the past 210 kyr linked to distant climate anomalies. Nature 432, 740–743.
Wang, Y.J., Cheng, H., Edwards, R.L., He, Y.Q., Kong, X.G., An, Z.S., Wu, J.Y., Kelly, M.J., Dykoski, C.A., Li, X., 2005. The Holocene Asian monsoon: links to solar changes and North Atlantic Climate. Science 308, 854–857.
Wang, Y.J., Cheng, H., Edwards, R.L., Kong, X.G., Shao, X.H., Chen, S.T., Wu, J.Y., Jiang, X.Y., Wang, X.F., An, Z.S., 2008. Millennial- and orbital-scale changes in the East Asian monsoon over the past 224,000 years. Nature 451, 1090–1093.
Wang, Y., Liu, X., Herzschuh, U., 2010. Asynchronous evolution of the Indian and east Asian summer monsoon indicated by Holocene moisture patterns in monsoonal central Asia. Earth Sci. Rev. 103, 135–153.
Webster, P.J., Magana, V.O., Palmer, T.N., Shukla, J., Tomas, R.A., Yanai, M.U., Yasunari, T., 1998. Monsoons: processes, predictability, and the prospects for prediction. J. Geophys. Res. 103, 14451–14510.

Wu, W.X., Liu, T.S., 2004. Possible role of the "Holocene Event 3" on the collapse of Neolithic Cultures around the Central Plain of China. Quat. Int. 117, 153–166.
Wu, J.Y., Wang, Y.J., Cheng, H., Kong, X.G., Liu, D.B., 2012. Stable isotope and trace element investigation of two contemporaneous annually-laminated stalagmites from northeastern China surrounding the "8.2 ka event". Clim. Past 8, 1497–1507.
Xiao, J.L., Nakamura, T., Lu, H.Y., Zhang, G.Y., 2002. Holocene climate changes over the desert/loess transition of north-central China. Earth Planet. Sci. Lett. 197, 11–18.
Xiao, J.L., Xu, Q.H., Nakamura, T., Yang, X.L., Liang, W.D., Inouchi, Y., 2004. Holocene vegetation variation in the Daihai Lake region of north-central China: a direct indication of the Asian monsoon climatic history. Quat. Sci. Rev. 23, 1669–1679.
Yamanaka, T., Shimada, J., Hamada, Y., Tanaka, T., Yang, Y.H., Zhang, W.J., Hu, C.S., 2004. Hydrogen and oxygen isotopes in precipitation in the northern part of the North China Plain: climatology and inter-storm variability. Hydrol. Process. 18, 2211–2222.
Yang, X., Scuderi, L., 2010. Hydrological and climatic changes in deserts of China since the late Pleistocene. Quat. Res. 73, 1–9.
Zhang, P.Z., Cheng, H., Edwards, R.L., Chen, F.H., Wang, Y.J., Yang, X.L., Liu, J., Tan, M., Wang, X.F., Liu, J.H., An, C.L., Dai, Z.B., Zhou, J., Zhang, D.Z., Jia, J.H., Jin, L.Y., Johnson, K.R., 2008. A test of climate, sun, and culture relationships from an 1810-year Chinese cave record. Science 322, 940–942.
Zhang, J.W., Chen, F.H., Holmes, J.A., Li, H., Guo, X.Y., Wang, J.L., Li, S., Lü, Y.B., Zhao, Y., Qiang, M.R., 2011. Holocene monsoon climate documented by oxygen and carbon isotopes from lake sediments and peat bogs in China: a review and synthesis. Quat. Sci. Rev. 30, 1973–1987.
Zhang, W.H., Wu, J.Y., Wang, Y., Wang, Y.J., Cheng, H., Kong, X.G., Duan, F.C., 2014. A detailed East Asian monsoon history surrounding the 'Mystery Interval' derived from three Chinese speleothem records. Quat. Res. 82, 154–163.
Zhao, Y., Yu, Z.C., Chen, F.H., Zhang, J.W., Yang, B., 2009. Vegetation response to Holocene climate change in monsoon-influenced region of China. Earth Sci. Rev. 97, 242–256.
Zhao, G.Y., Liu, X.M., Chen, Q., Lu, B., Niu, H.W., Liu, Z., Li, P.Y., 2013. Paleoclimatic evolution of Holocene loess and discussion of the sensitivity of magnetic susceptibility and median diameter. Quat. Int. 296, 160–167.